Cellular and Molecular Life Sciences (2023) 80:167
https://doi.org/10.1007/s00018-023-04813-9

ORIGINAL ARTICLE

Cell density-dependent membrane distribution of ganglioside GM3 in melanoma cells

Motohide Murate[1,2,3] · Noriko Yokoyama[4] · Nario Tomishige[1,2,3] · Ludovic Richert[2] · Nicolas Humbert[2] · Brigitte Pollet[2] · Asami Makino[1,5] · Nozomu Kono[6] · Laura Mauri[7] · Junken Aoki[6] · Yasushi Sako[3] · Sandro Sonnino[7] · Naoko Komura[8] · Hiromune Ando[8] · Mika K. Kaneko[9] · Yukinari Kato[9] · Kei-ichiro Inamori[10] · Jin-ichi Inokuchi[10,11] · Yves Mély[2] · Kazuhisa Iwabuchi[4] · Toshihide Kobayashi[1,2,3]

Received: 20 January 2023 / Revised: 21 April 2023 / Accepted: 17 May 2023

Abstract

Monosialoganglioside GM3 is the simplest ganglioside involved in various cellular signaling. Cell surface distribution of GM3 is thought to be crucial for the function of GM3, but little is known about the cell surface GM3 distribution. It was shown that anti-GM3 monoclonal antibody binds to GM3 in sparse but not in confluent melanoma cells. Our model membrane study evidenced that monoclonal anti-GM3 antibodies showed stronger binding when GM3 was in less fluid membrane environment. Studies using fluorescent GM3 analogs suggested that GM3 was clustered in less fluid membrane. Moreover, fluorescent lifetime measurement showed that cell surface of high density melanoma cells is more fluid than that of low density cells. Lipidomics and fatty acid supplementation experiment suggested that monounsaturated fatty acid-containing phosphatidylcholine contributed to the cell density-dependent membrane fluidity. Our results indicate that anti-GM3 antibody senses GM3 clustering and the number and/or size of GM3 cluster differ between sparse and confluent melanoma cells.

Keywords Anti-ganglioside antibodies · Crypticity · Fluorescence lifetime imaging · Lipidomics · Plasma membrane

Abbreviations

Chol	Cholesterol
DMPC	1,2-Dimyristoyl-*sn*-glycero-3-phosphocholine
DOPC	1,2-Dioleoyl-*sn*-glycero-3-phosphocholine

Toshihide Kobayashi: Lead contact.

✉ Motohide Murate
mmurate@riken.jp

✉ Kazuhisa Iwabuchi
iwabuchi@juntendo.ac.jp

✉ Toshihide Kobayashi
toshihide.kobayashi@unistra.fr

1 Lipid Biology Laboratory, RIKEN, Wako, Saitama 351-0198, Japan

2 Laboratoire de Bioimagerie et Pathologies, UMR 7021, CNRS, Faculté de Pharmacie, Université de Strasbourg, 67401 Illkirch, France

3 Cellular Informatics Laboratory, RIKEN CPR, Wako, Saitama 351-0198, Japan

4 Institute for Environmental and Gender-Specific Medicine, Graduate School of Medicine, Juntendo University, Urayasu, Chiba 279-0021, Japan

5 Molecular Physiology Laboratory, RIKEN CPR, Wako, Saitama 351-0198, Japan

6 Department of Health Chemistry, Graduate School of Pharmaceutical Sciences, The University of Tokyo, 7-3-1, Hongo, Bunkyo-Ku, Tokyo 113-0033, Japan

7 Department of Medical Biotechnology and Translational Medicine, University of Milan, Milan, Italy

8 Institute for Glyco-Core Research, Gifu University, 1-1 Yanagido, Gifu 501-1193, Japan

9 Department of Antibody Drug Development, Tohoku University Graduate School of Medicine, Sendai, Miyagi 980-8575, Japan

10 Division of Glycopathology, Institute of Molecular Biomembrane and Glycobiology, Tohoku Medical and Pharmaceutical University, Sendai 981-8558, Japan

11 Forefront Research Center, Graduate School of Science, Osaka University, Toyonaka, Osaka 560-0043, Japan

Published online: 30 May 2023

DPPC	1,2-Dipalmitoyl-*sn*-glycero-3-phosphocholine
EGFR	Epidermal growth factor receptor
F2N12S	N-[[4'-N,N-diethylamino-3-hydroxy-6-flavonyl]-methyl]-N-methyl-N-(3-sulfopropyl)-1-dodecanaminium: inner salt
FLIM	Fluorescence lifetime imaging microscopy
FRET	Förster resonance energy transfer
GlcCer	Glucosylceramide
GM1	Ganglioside GM1
GM3	Monosialoganglioside GM3 (NeuAcα3Galβ-4Glcβ1Cer)
Ld	Liquid-disordered
Lo	Liquid-ordered
MDCK	Madin-Darby canine kidney
NPA	Niemann-pick A
POPC	1-Palmitoyl-2-oleoyl-*sn*-glycero-3-phosphocholine
pSM	Palmitoyl sphingomyelin
SM	Sphingomyelin
SPR	Surface plasmon resonance

Introduction

Monosialoganglioside GM3 (NeuAcα3Galβ-4Glcβ1Cer) is the simplest ganglioside. GM3 is distributed in various mammalian cells and tissues and is involved in multiple cellular signaling by modulating the activities of integrin [1], insulin receptor [2] and epidermal growth factor receptor (EGFR) [3, 4]. It is postulated that cell surface distribution of GM3 is crucial for its function [5]. Monoclonal anti-GM3 antibodies [6–8] and polyclonal anti-GM3 antibodies from patients [9] have been used to examine cellular GM3 distribution. These antibodies revealed heterogeneous distribution of GM3-rich domains on the plasma membrane of human T cells [9], Madin-Darby canine kidney (MDCK) cells [10] and mouse fibroblasts [11]. It was also demonstrated that GM3-rich domains were distinct from caveolae in MDCK cells [12].

Anti-ganglioside antibodies are believed to be a crucial pathogenic factor of peripheral nerve diseases [13]. It is well recognized that antigen gangliosides are often cryptic [14]. "Cryptic glycolipids" are the cell surface glycolipids that are not accessible to proteins such as anti-glycolipid antibodies or sialidases. This makes the evaluation of pathogenic antibodies and determination of ganglioside distribution difficult. Currently, two mechanisms are reported for the ganglioside crypticity: (1) steric hindrance by other gangliosides for the binding of anti-GM3 [15] and anti-GM1 [16] antibodies and (2) cholesterol-induced conformation change of GM1 [17]. It is not known whether other mechanism(s) might also be involved in ganglioside crypticity.

Previously, it was shown that anti-GM3 antibody labeled sparse but not high density B16 melanoma cells [18]. Similar results were obtained in hamster embryo fibroblasts [18] and glioma cells [19]. These cells contain GM3 as a single ganglioside. Cell density did not affect cellular GM3 content [18] but may affect its distribution in sparse and confluent melanoma and glioma cells. Surface labeling of GM3 in glioma cells by sodium [^{3}H] borohydride after sodium peroxide treatment indicated that cell surface GM3 was equally labeled in sparse and confluent cells [19]. These results indicate that GM3 is cryptic in confluent melanoma and glioma cells and suggest different membrane organization of GM3 in sparse and confluent melanoma cells.

In this study, we investigated the interaction of monoclonal anti-GM3 antibodies with GM3 in different membrane environments using model membranes and cultured cells. Our results indicate that the antibodies preferentially bind to GM3 clusters. Formation of GM3 cluster is dependent on membrane fluidity and the plasma membrane is more fluid in confluent melanoma cells as compared to sparse cells. Thus, our studies revealed a cell density-dependent alteration of membrane organization of GM3.

Results

Binding of anti-GM3 antibody to GM3/partner lipid is dependent on incubation temperatures and phase transition temperatures of partner lipids

Mouse monoclonal IgM against GM3 (clone GMR6) established by Kotani et al. [7] by immunizing purified GM3, has been widely employed to label cellular GM3 [10–12, 20–25]. We first characterized this antibody in depth using model systems. In Fig. 1A, the binding of the antibody to various lipids was compared. The antibody strongly bound to milk GM3 (GM3) and to a lesser extent to GM2. The antibody did not significantly bind to other glycolipids or phospholipids, including lyso GM3.

In Fig. 1B, GM3 was mixed with 1,2-dioleoyl-*sn*-glycero-3-phosphocholine (DOPC, Gel to liquid crystalline phase transition temperature, $T_m = -17$ ℃), 1-palmitoyl-2-oleoyl-*sn*-glycero-3-phosphocholine (POPC, $T_m = -2$ ℃), 1,2-dimyristoyl-*sn*-glycero-3-phosphocholine (DMPC, $T_m = 24$ ℃) and 1,2-dipalmitoyl-*sn*-glycero-3-phosphocholine (DPPC, $T_m = 41$ ℃) [26] and the binding of the anti-GM3 antibody was measured at 4 ℃, room temperature (23 ℃), 37 ℃ or 42 ℃ by ELISA. The antibody efficiently bound GM3/DPPC (1:9) at 4 ℃ and room temperature. The binding was drastically decreased at 37 ℃ and 42 ℃. Although the binding was less efficient, binding to GM3/DMPC (1:9) and GM3/POPC (1:9) also showed temperature dependence. The antibody did not significantly bound

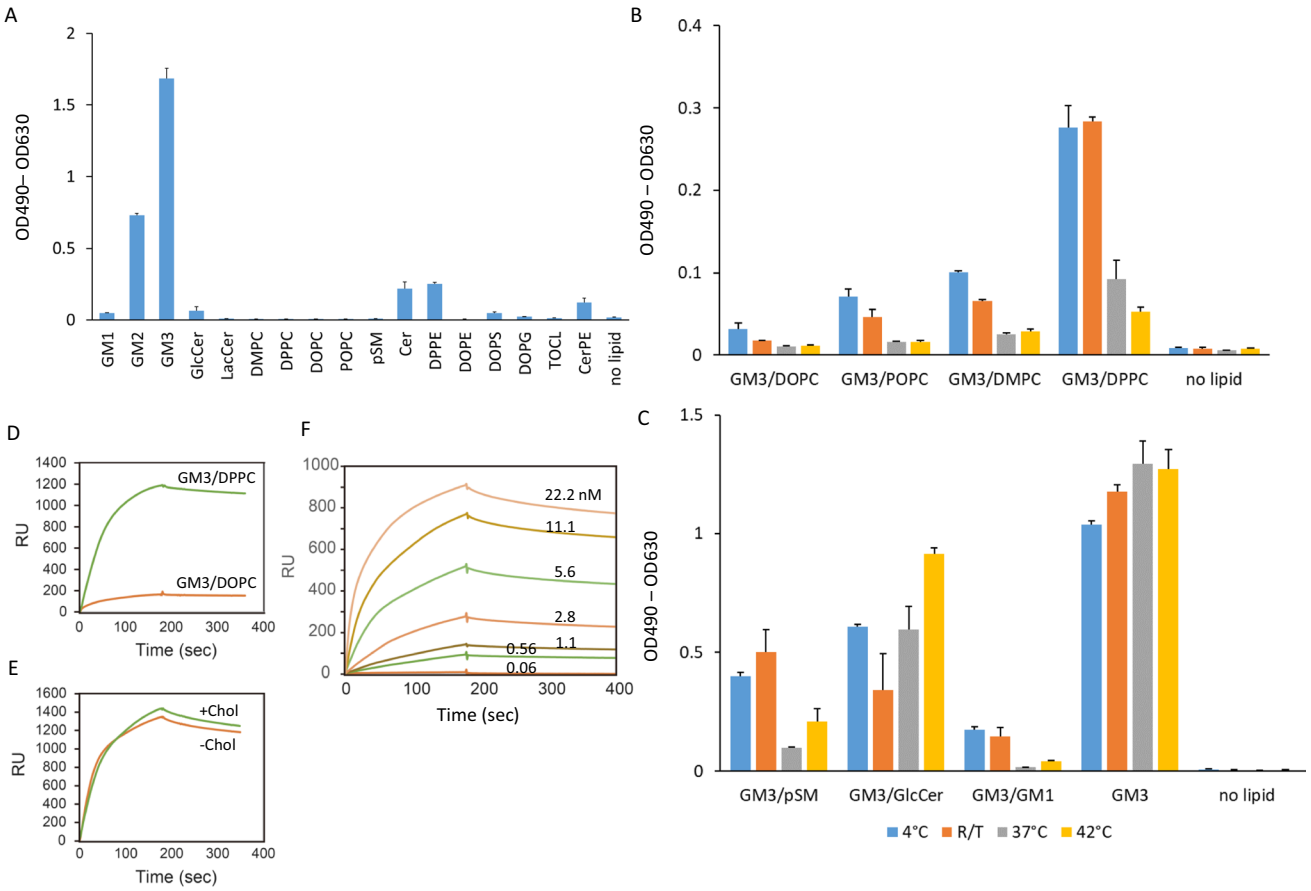

Fig. 1 Binding of anti-GM3 antibody (GMR6) to GM3/partner lipid is dependent on incubation temperatures and phase transition temperatures of partner lipids. **A** Binding of 0.37 μg/mL of anti-GM3 antibody to indicated lipids (0.5 nmol/well) was measured by ELISA. GM1, ganglioside GM1; GM2, ganglioside GM2; GM3, ganglioside GM3; GlcCer, glucosylceramide; LacCer, lactosylceramide; DMPC, 1,2-dimyristoyl-*sn*-glycero-3-phosphocholine; DPPC, 1,2-dipalmitoyl-*sn*-glycero-3-phosphocholine; DOPC, 1,2-dioleoyl-*sn*-glycero-3-phosphocholine; POPC, 1-palmitoyl-2-oleoyl-*sn*-glycero-3-phosphocholine; pSM, palmitoyl sphingomyelin;Cer, ceramide; DPPE, 1,2-dipalmitoyl-*sn*-glycero-3-phosphoethanolamine; DOPE, 1,2-dioleoyl-*sn*-glycero-3-phosphoethanolamine; DOPS, 1,2-dioleoyl-*sn*-glycero-3-phospho-L-serine; DOPG, 1,2-dioleoyl-*sn*-glycero-3-phospho-(1'-rac-glycerol); TOCL, 1',3'-bis[1,2-dioleoyl-*sn*-glycero-3-phospho]-glycerol; CerPE, N-acyl-sphingosylphosphorylethanolamine. **B** Binding of 0.37 μg/mL of anti-GM3 antibody to GM3/DOPC (1:9), GM3/POPC (1:9), GM3/DMPC (1:9) or GM3/DPPC (1:9) (0.5 nmol GM3/well) at indicated temperature measured by ELISA. **(C)** Binding of 0.37 μg/mL of anti-GM3 antibody to GM3/pSM (1:9), GM3/GlcCer (1:9), GM3/GM1 (1:9) or GM3 alone (0.5 nmol GM3/well) at indicated temperatures measured by ELISA. Data in **A**–**C** are means ± SD of three experiments. **D** Binding of anti-GM3 antibody (10 ng/mL) to GM3/DOPC (1:5) (orange) or GM3/DPPC (1:5) (green) liposomes measured by surface plasmon resonance (SPR). SPR was performed as described in Methods. **E** Binding of anti-GM3 antibody to DPPC/GM3 (5:2) (orange) or DPPC/GM3/Chol (5:2:5) (green) liposomes. **F** Binding of different concentration of anti-GM3 antibody to GM3/DPPC (1:9) liposomes

to GM3/DOPC (1:9). In Fig. 1C, we examined the effect of palmitoyl sphingomyelin (pSM, $T_m = 40$ °C), glucosylceramide (GlcCer, $T_m = 66$–68 ℃) and ganglioside GM1 (GM1, $T_m = \sim 20$ ℃) [26] on the antibody binding when mixed with GM3. Binding to GM3/pSM (1:9) and GM3/GM1 (1:9) showed similar results to those of GM3/DPPC and GM3/DMPC. In contrast, the binding to GM3/GlcCer (1:9) did not show clear temperature dependence between 4 and 42 ℃. Binding to pure GM3 ($T_m = 35$–40 ℃) [26] also did not show temperature dependence (Fig. 1C). These results indicate that the binding of anti-GM3 antibody to GM3-containing lipid mixture is dependent on the physical properties of the partner lipids and that gel phase lipids give higher binding than liquid crystalline lipids. In Suppl. Fig. 1, we measured binding of anti-GM3 antibody to synthetic GM3s (sphingosine backbone C18:1, fatty acid composition C8:0 to C24:0). The antibody bound efficiently to C16:0 GM3 and C24:0 GM3. Binding was decreased in C12:0 GM3. The antibody did not bind to C8:0 GM3. Similar to milk GM3, in C12:0 GM3 to C24:0 GM3, the antibody bound to GM3/DPPC (1:9) more efficiently than GM3/POPC (1:9).

We then compared the binding of other established anti-GM3 monoclonal antibodies to GM3/DPPC and GM3/DOPC. Anti-GM3 IgM monoclonal antibody M2590 was

established after immunization of C57BL/6 mice with syngenic B16 melanoma cells [6, 27]. Anti-GM3 IgG monoclonal antibody DH2 was originally established after immunization of C57BL/6 mice with GM3 lactone coated on *Salmonella minnesotae* [8]. The DH2 antibody is a mouse IgG_3 known as a highly sensitive and specific antibody against GM3. However, in recent years, antibody production from DH2 hybridoma has become unstable, and the activity of purified antibody has been low. Therefore, we cloned the antibody gene from the DH2 hybridoma and constructed expression plasmids for the H and L chains. The recombinant DH2 (recDH2) antibody purified from supernatant culture of CHO/recDH2 cells was used for binding study.

Both antibodies showed higher binding to GM3/DPPC and lower binding to GM3/DOPC (Suppl. Fig. 2). These results indicate that the partner lipid-dependent binding to GM3 is a common property of anti-GM3 antibodies. We used GMR6 antibody in the following experiments.

Next, we examined the binding of the antibody to immobilized lipid bilayers containing GM3 by surface plasmon resonance (SPR) (Fig. 1D–F). As observed in ELISA, the binding of GMR6 antibody was significantly different between GM3/DPPC and GM3/DOPC (Fig. 1D). Previously, the binding of cholera toxin B-subunit to GM1 was shown to be inhibited by cholesterol (Chol) [17]. Thus we added Chol to GM3/DPPC liposomes. The addition of Chol did not affect the binding of the antibody to GM3 (Fig. 1E). Consistent with SPR results, presence of Chol did not inhibit the antibody binding to GM3 in ELISA (Suppl. Figure 3). These results suggest that the molecular mechanism of GM3/DOPC crypticity against anti-GM3 antibody is different from that of GM1/Chol to cholera toxin. From Fig. 1F the dissociation constant K_D of GMR6 antibody to GM3/DPPC (1:9) was calculated to be $2.8 \pm 0.8 \times 10^{-10}$ M ($n = 4$). The binding of the antibody to GM3/DOPC was too low to obtain reliable K_D value.

Fluorescent GM3 analogs form clusters in DPPC

To examine the difference of GM3 distribution in DPPC and DOPC membranes, we employed two fluorescent GM3 analogs, C11 TopFluor-GM3 and ATTO594-GM3 [28] (Suppl Fig. 4). Fluorescent lipid analogs exhibit self-quenching in a concentration-dependent manner [29, 30]. There is little self-quenching if small amount of a fluorescent lipid is well mixed with bulk membrane lipids. In contrast, when a fluorescent lipid is excluded from bulk lipids, fluorescent lipid forms clusters and thus is self-quenched [31, 32]. Solubilization of lipids by detergent dilutes fluorescent lipid clusters in detergent micelles and thus dequenches fluorescence. We first measured emission spectra of DOPC/C11 TopFluor-GM3 (99.5/0.5 mol/mol) (Fig. 2A) and DPPC/C11 TopFluor-GM3 (99.5/0.5 mol/mol) (Fig. 2B) in the absence and presence of 1% Triton X-100 at 20 ℃. C11 TopFluor-GM3 was quenched 21% in DOPC and 44% in DPPC. Comparison of Fig. 2A and B shows that even in the presence of Triton X-100, the fluorescence intensity of DOPC/C11 TopFluor-GM3 is higher than that of DPPC/C11 TopFluor-GM3. This may be due to the partial insolubility of DPPC in Triton X-100 [33]. Thus we may underestimate the quenching efficiency of C11 TopFluor-GM3 in DPPC. These results suggest that in both DOPC and DPPC, TopFluor is clustered. However, the number and/or size of clusters are larger in DPPC.

There is an overlap in the emission spectrum of C11 TopFluor-GM3 and the absorption spectrum of ATTO594-GM3. Thus we can expect Förster resonance energy transfer (FRET) between the two lipids when they are in close proximity. Figure 2C and D show emission spectra of DOPC and DPPC liposomes containing 0.5 mol% C11 TopFluor-GM3 and 0.5 mol% ATTO594-GM3, respectively, in the absence and presence of 1% Triton X-100 at 20 ℃. Appearance of 630 nm peak in the absence of Triton X-100 indicates FRET between C11 TopFluor-GM3 and ATTO594-GM3. Calculation of fluorescence intensity at 507 nm in the presence and absence of FRET acceptor, ATTO594-GM3, in the absence of Triton X-100 using Eq. (1) indicates that FRET efficiency is 64% in DOPC and 82% in DPPC. We then measured self-quenching of ATTO594-GM3 in these liposomes by measuring fluorescence from 605 to 700 nm at excitation 603 nm in the presence and absence of Triton X-100 (Fig. 2E and F). ATTO594-GM3 was self-quenched 10% in DOPC and 50% in DPPC. Similar to Fig. 2A and B, fluorescence intensity of DPPC/ATTO594-GM3 showed lower fluorescence than DOPC/ATTO594-GM3 in the presence of Triton X-100. Increased self-quenching of ATTO594-GM3 and increased FRET in DPPC suggest that DPPC enhanced clustering of GM3 analogs.

We then measured emission spectra of DOPC/C11 TopFluor-GM3/ATTO594-GM3 (99/0.5/0.5 mol/mol/mol) (Fig. 2G) and DPPC/C11 TopFluor-GM3/ATTO594-GM3 (99/0.5/0.5 mol/mol/mol) (Fig. 2H) in the absence of 1% Triton X-100 at different temperatures. In DPPC, FRET signal was higher at 4 ℃ and 20 ℃ compared to 37 ℃ and 42 ℃ (Fig. 2H–J). In contrast, DOPC did not show temperature-dependent FRET. We then examined whether ATTO594-GM3, the FRET acceptor alone shows temperature-dependent fluorescence in DPPC. Figure 2K and L show emission spectra of DOPC and DPPC liposomes containing 0.5% ATTO594-GM3 with excitation at 603 nm at different temperatures. ATTO594-GM3 did not show temperature-dependent fluorescence both in DOPC and DPPC. This suggests that the number and/or size of fluorescent GM3 analog clusters were increased at lower temperatures in DPPC.

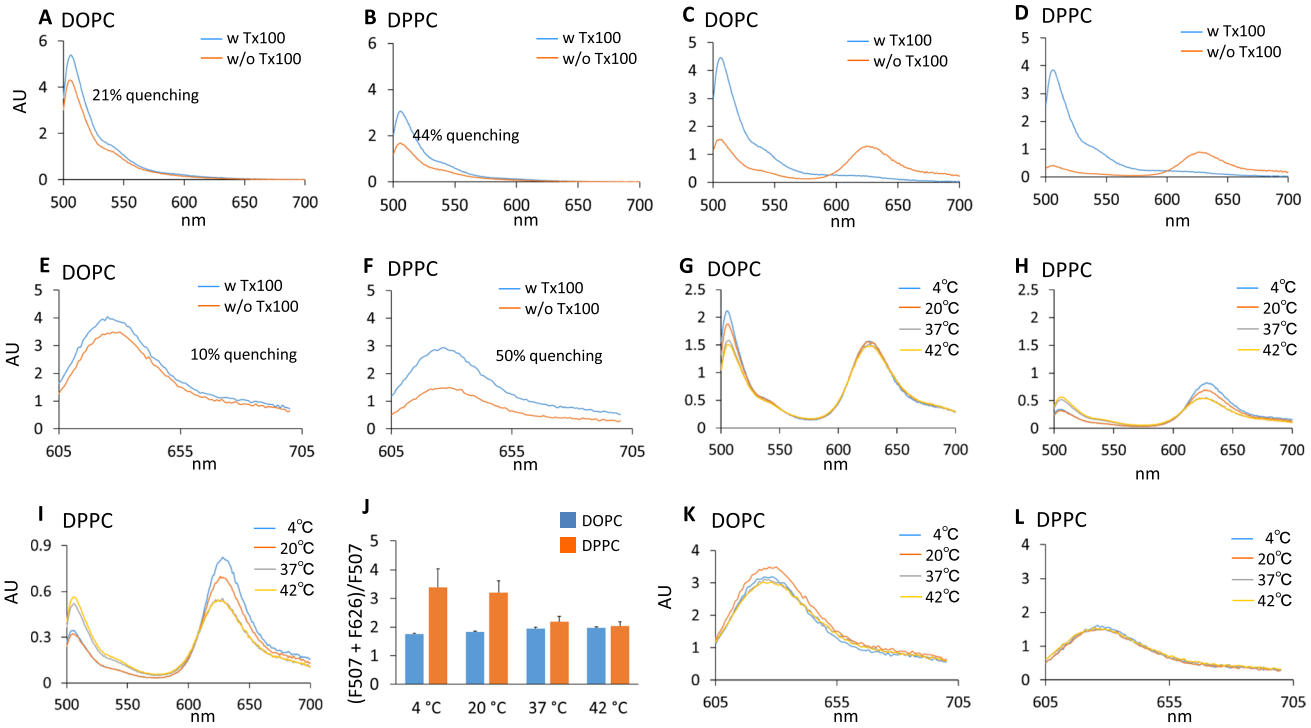

Fig. 2 Fluorescent GM3 analogs form clusters in DPPC. **A, B** Emission spectra of DOPC/C11 TopFluor GM3 (99.5/0.5 mol/mol) (**A**) or DPPC/C11 TopFluor-GM3 (99.5/0.5 mol/mol) (**B**) liposomes in the presence and absence of Triton X-100 at 20 °C. Liposomes were prepared as described in Methods. Excitation at 495 nm. **C**, **D** Emission spectra of DOPC/C11 TopFluor-GM3/ATTO594 GM3 (99/0.5/0.5 mol/mol/mol) (**C**) or DPPC/C11 TopFluor-GM3/ATTO594-GM3 (99/0.5/0.5 mol/mol/mol) **(D)** liposomes in the presence and absence of Triton X-100 at 20 °C. Excitation at 495 nm. **E**, **F** Emission spectra of DOPC/C11 TopFluor GM3/ATTO594 GM3 (99/0.5/0.5 mol/mol/mol) (**E**) or DPPC/C11 TopFluor-GM3/ATTO594-GM3 (99/0.5/0.5) (**F**) liposomes in the presence and absence of Triton X-100 at 20 ℃. Excitation at 603 nm. **G-I** Emission spectra of DOPC/C11 TopFluor-GM3/ATTO594-GM3 (99/0.5/0.5) (**G**) or DPPC/C11 TopFluor-GM3/ATTO594-GM3 (99/0.5/0.5 mol/mol/mol) (**H, I**) liposomes at different temperatures. Excitation at 495 nm. Spectra in **H** were enlarged in **I**. **J** FRET efficiency of (**G**) and (**H**) were calculated by Eq. (2). Data are means ± SD of three experiments. **K**, **L** Emission spectra of DOPC/C11 TopFluor-GM3/ATTO594-GM3 (99/0.5/0.5 mol/mol/mol) (**K**) or DPPC/C11 TopFluor-GM3/ATTO594-GM3 (99/0.5/0.5 mol/mol/mol) **(L)** liposomes at various temperatures. Excitation at 603 nm

Cell density dependent labeling of cellular GM3 by anti-GM3 antibody

Figure 1 suggests that anti-GM3 antibody labels cellular GM3 in a temperature-dependent manner. In Suppl. Fig. 5, various cells were fixed and cell surface GM3 was labeled with anti-GM3 antibody at different temperatures. It is reported that lipids are not fixed by PFA [34]. All cells tested were efficiently labeled at 4 ℃. However, labeling was decreased at higher temperatures. Different cells showed different labeling temperature thresholds. Human embryonic kidney cell line, HEK293, was labeled at 4 ℃ and room temperature, but not at 37 ℃ and 42 ℃. On the other hand, mouse melanoma cell line, MEB4 was labeled at 37 ℃ but not at 42 ℃. In Suppl. Fig. 5C, the antibody was incubated at 42 ℃ for 30 min before labeling MEB4 cells at 4 ℃. Suppl. Fig. 5C indicates that the antibody was not inactivated at 42 ℃. Interestingly, normal human skin fibroblast and skin fibroblast from Niemann-Pick A (NPA) patient showed different temperature dependence. NPA is a genetic defect of acid SMase characterized by the accumulation of SM in late endosomes/lysosomes [35]. Our results suggest altered GM3 clustering of the plasma membranes between normal and NPA fibroblasts.

Previously it was shown that anti-GM3, M2590, labeled sparse but not high density mouse melanoma cells [18]. In Fig. 3A and B, we labeled sparse and high density MEB4 cells by anti-GM3 antibody, GMR6. The antibody labeled low density melanoma cells as described in Suppl. Fig. 5. Similar to M2590, GMR6 antibody did not label high density melanoma cells even at 4 ℃.

Model lipid experiments in Fig. 2 suggest that the observed difference of anti-GM3 labeling in sparse and confluent melanoma cells may be due to the altered lipid order in the plasma membranes. To validate this hypothesis, we employed N-[[4'-N,N-diethylamino-3-hydroxy-6-flavonyl]-methyl]-N-methyl-N-(3-sulfopropyl)-1-dodecanaminium, inner salt (F2N12S) [36] to compare the membrane order

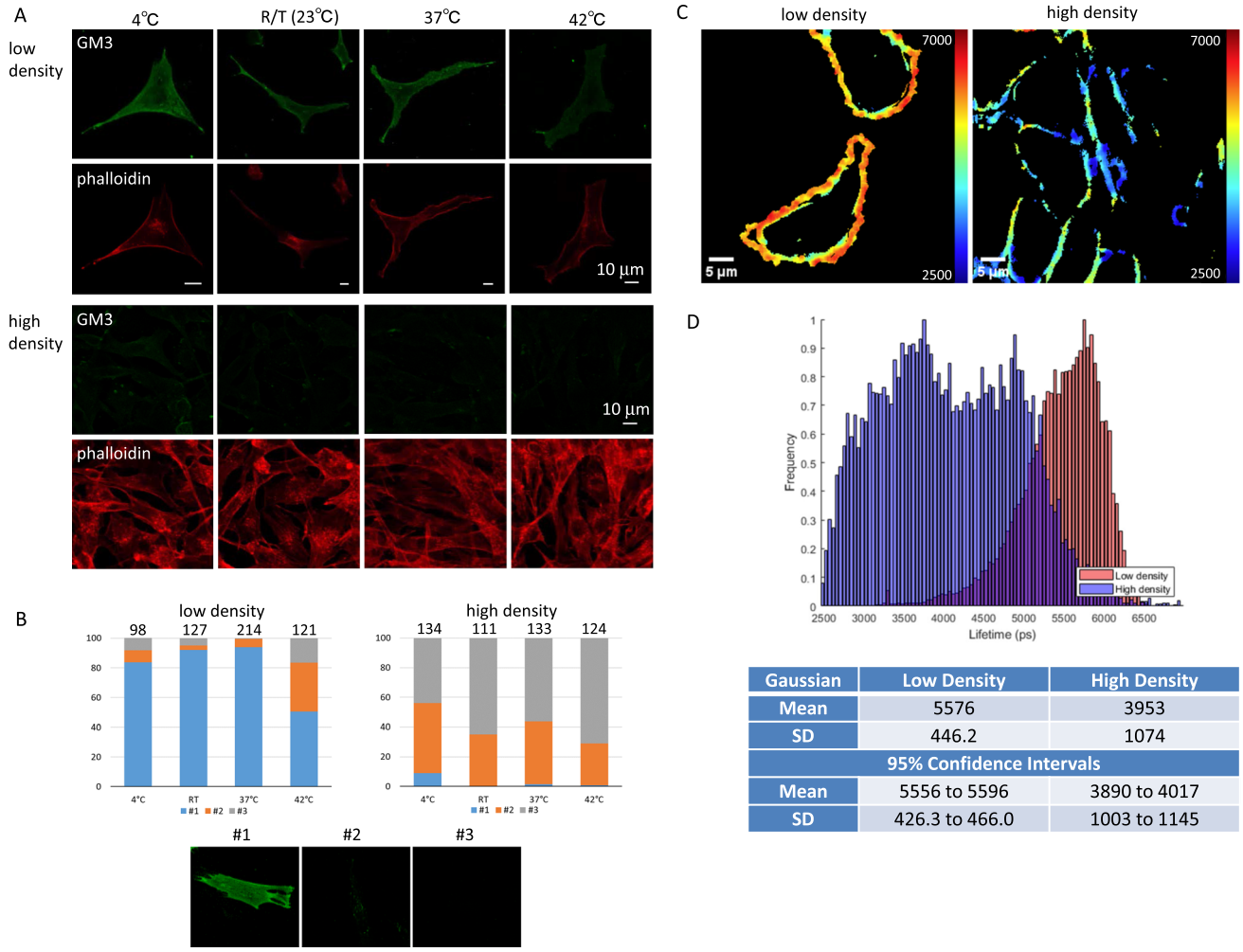

Gaussian	Low Density	High Density
Mean	5576	3953
SD	446.2	1074
95% Confidence Intervals		
Mean	5556 to 5596	3890 to 4017
SD	426.3 to 466.0	1003 to 1145

Fig. 3 Cell density dependent labeling of cellular GM3 by anti-GM3 antibody. **A** Low density ($1.4 \pm 0.4 \times 10^4$ cells/15 mmϕ coverslip ($n=3$)) and high density ($2.8 \pm 0.6 \times 10^5$ cells/15 mmϕ coverslip ($n=4$)) MEB4 cells were fixed and labeled with anti-GM3 antibody as described in Methods. Cells were doubly labeled with phalloidin to identify cells. **B** Distribution of cells with different labeling at different temperatures. #1, whole cells were labeled; #2, only a part of cells were labeled. #3, no labeling. The numbers on the top of the bars are number of cells counted. **C** FLIM images of low density and high density MEB4 cells labeled with F2N12S at 25 ℃. Cells were labeled as described in Methods. The pixel colors describe the lifetime values in picosecond according to the color scale on the Y axis. **D** Lifetime distribution for low and high density cells. The data in the table are the mean and standard deviation of the average lifetime obtained with the 12 images taken individually. Two-photon excitation was at 830 nm and fluorescence was collected through a band-pass filter 585 nm

between sparse and confluent MEB4. Being conjugated to a zwitter ion headgroup and a long alkyl chain, the two-color F2N12S fluorophore is selectively anchored at the plasma membrane outer leaflet [36]. Our previous data showed that the long-lived and mean lifetimes of the tautomer (T*) band of F2N12S differ by a factor of 2 between liquid-ordered (Lo) and liquid-disordered (Ld) phases, and thus can be used by fluorescence lifetime imaging microscopy (FLIM) to sensitively and straightforwardly monitor the changes in lipid phase in cells [37]. Figure 3C and D compare the FLIM images of low density and high density MEB4 cells. FLIM of low density cells showed homogeneous distribution of lifetimes, exhibiting a mean lifetime value 5.6 ± 0.4 ns. This value was significantly decreased in high density cells (4.0 ± 1.0 ns), indicating a decrease in the lipid order in confluent cells.

Lipidomics indicates a different composition of phospholipids in sparse and confluent melanoma cells

Since F2N12S selectively labels the outer leaflet of the plasma membrane, the decrease of lipid order in high density MEB4 cells suggests that the lipid composition of the outer leaflet may differ between high density and low density cells. Lipid order of the outer leaflet of the

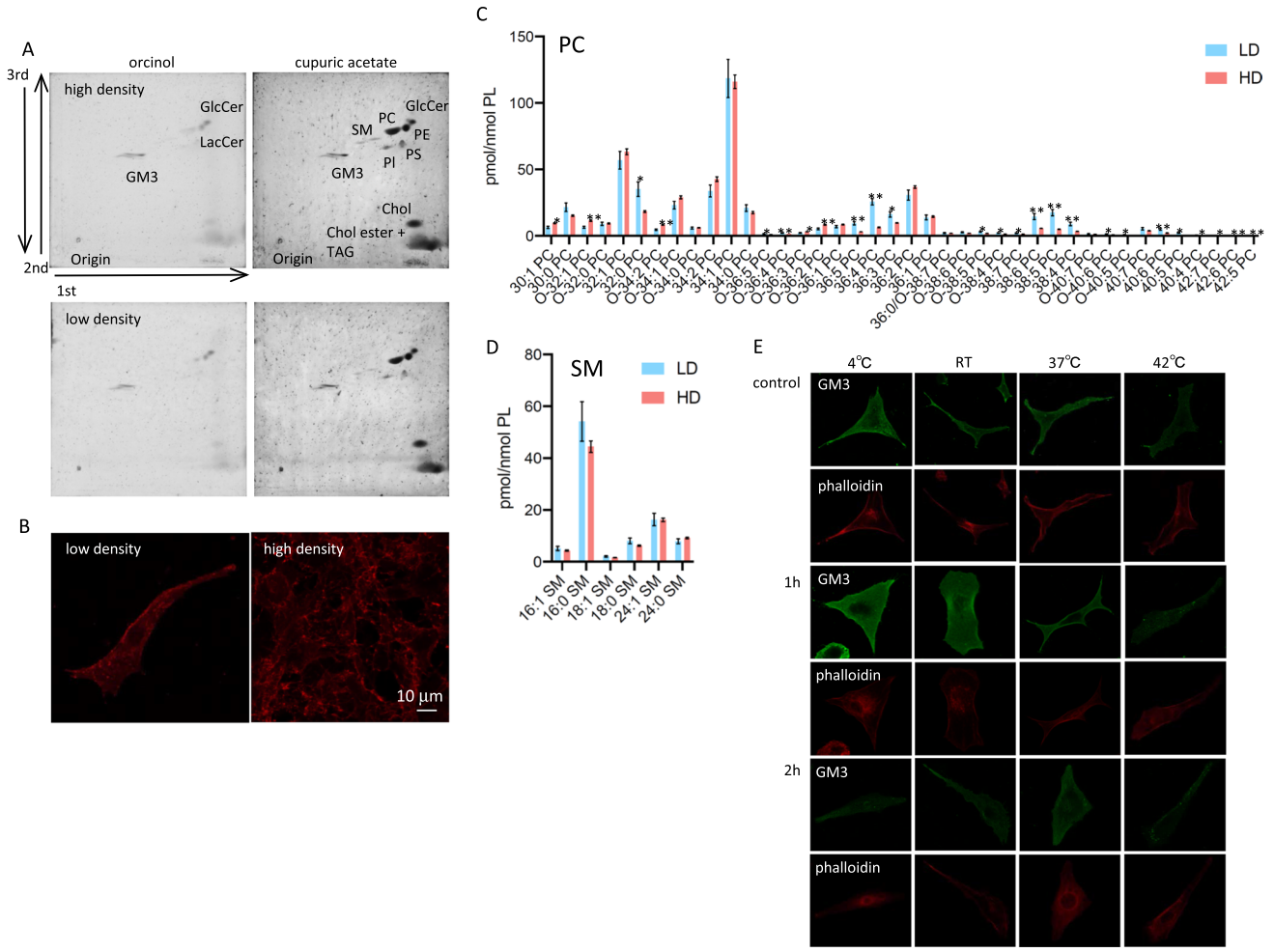

Fig. 4 Different composition of phospholipid molecular species in sparse and confluent melanoma cells. **A** 2D-HPTLC analysis of lipid composition of low density and high density MEB4 cells. 2D-HPTLC was performed as described in Methods. **B** Cell surface labeling of low density and high density cells with mCherry-D4. **C**, **D** Lipidomics analyses of phosphatidylcholine (PC) **(C)** and sphingomyelin (SM) **(D)** from low density and high density cells. Lipidomics was performed as described in Methods. Data in **C** and **D** are mean ± SD of three experiments. $*P<0.05$, $**P<0.01$. **(E)** Anti-GM3 antibody labeling of low density MEB4 cells treated with oleic acid. Oleic acid treatment was performed as described in Methods

plasma membrane is sensitive to the content of cholesterol, sphingolipids, unsaturated fatty acids and saturated fatty acids. Figure 4A shows the results of 2D-HPTLC analysis of lipids extracted from low density and high density MEB4 cells. Orcinol labeling revealed glycolipids, whereas cupric acetate labeled all lipids. Figure 4A indicates that gross lipid composition was not significantly different between low density and high density cells. This is supported by the observation that cell surface cholesterol-rich domains labeled with mCherry-D4 [38, 39] did not significantly differ between low density and high density cells (Fig. 4B).

We then examined different molecular species of phospholipids by lipidomics (Fig. 4C, D and Suppl. Figure 6). There was no significant difference in content and molecular species of sphingomyelin (SM) between low density and high density cells (Fig. 4D). In contrast, significant decrease of DPPC (32:0 PC), increase of several mono- and di-unsaturated molecular species (30:1 PC, O-32:1 PC, O-34:2 PC and O-36:2 PC) and decrease of polyunsaturated PCs were observed (Fig. 4C). Increase of mono- or di-unsaturated molecular species and decrease of polyunsaturated molecular species in high density cells were also observed in phosphatidylethanolamine and phosphatidylinositol (Suppl Fig. 6). In phosphatidylserine, both saturated and unsaturated molecular species were decreased in high density cells (Suppl Fig. 6).

Phospholipids are asymmetrically distributed in the plasma membrane [25, 40, 41], the outer leaflet of the plasma membrane is enriched with phosphatidylcholine

and sphingomyelin. Since there were no significant differences in sphingomyelin molecular species between low density and high density melanoma cells, sphingomyelin may not contribute to the observed alteration of lipid order in high density cells. Fatty acid composition of phosphatidylcholine in the outer leaflet of nucleated cells is not fully understood. However, analysis of lipid composition of envelope viruses bud from different plasma membrane domains suggests the enrichment of monounsaturated phosphatidylcholine in the plasma membrane of human skin fibroblasts [42]. Our results showed the increase of monounsaturated phosphatidylcholine in high density cells, suggesting that the increase of monounsaturated phosphatidylcholine is responsible for the decreased lipid order in high density cells.

We then examined whether the addition of monounsaturated fatty acid, oleic acid (C18:1) to low density cells mimic high density cells. Exogenously added oleic acid is rapidly incorporated to cells [43]. Oleic acid stimulates lipid droplet formation by activating the long-chain fatty acid receptor FFAR4 [44]. Results of fluorescent fatty acid analogs suggest that the exogenously added fatty acids are accumulated to lipid droplets [45, 46] in which neutral lipids, triglyceride and cholesterol ester are enriched. In addition to neutral lipids, oleic acid is incorporated into phospholipids. In HepG2 cells, oleic acid is mainly incorporated to phosphatidylcholine (8 nmol/mg protein after 2 h) and triglyceride (6 nmol/mg) followed by phosphatidylethanolamine (3 nmol/mg) [47]. Efficient incorporation of oleic acid to phosphatidylcholine is reported in other cell types [48–51]. Anti-GM3 labeling became very dim after 2 h incubation of low density cells with oleic acid (Fig. 4E). These results suggest that an alteration of fatty acid composition in high density cells is the cause of decreased anti-GM3 labeling and the differences in GM3 microenvironment as compared to low density melanoma cells.

Discussion

Partner lipid-dependent binding to GM3 is a common property of anti-GM3 antibodies

In this study, we examined binding of three independently-isolated anti-GM3 monoclonal antibodies to DOPC/GM3 and DPPC/GM3. All three antibodies showed preference to DPPC/GM3, suggesting that partner lipid-dependent binding to GM3 is a common characteristic of anti-GM3 antibodies. The binding of GMR6 antibody to GM3 in ELISA was dependent on the gel-to-liquid crystalline phase transition temperature of partner lipids and incubation temperature, showing higher binding in gel phase lipids than in liquid crystalline phase lipids. In contrast, the binding to GM3 alone was not affected by incubation temperature. The binding of GMR6 antibody is dependent on the chain lengths of the fatty acyl chain of GM3 and the antibody did not significantly bind to lyso GM3. These results suggest that the antibody recognizes both hydrophilic headgroup and hydrophobic ceramide moiety of GM3. Since GM3 forms clusters in DPPC, our results suggest that the epitope of the antibody may be both aggregated sugar and ceramide moiety of GM3.

GM3 is clustered in DPPC

Our liposome experiments with fluorescent GM3 analogs indicate that GM3 analogs were highly aggregated in DPPC. Thus, our results suggest that anti-GM3 antibodies bind clustered GM3. Aggregation of GM3 in DPPC is consistent with previous small-angle X-ray diffraction observation that GM3 and DPPC are phase separated [52, 53]. Whereas more complicated gangliosides form micelles, GM3 forms bilayers. The main phase transition of GM3 is reported to be 35–40 ℃ [26, 54]. This is very close to the phase transition temperature of DPPC (T_m = 41 ℃) [26]. In contrast to GM3, palmitoyl (C16:0) SM (pSM) (T_m = 40 ℃) [26] forms clusters in DOPC and is well mixed with DPPC [55]. In contrast to pSM, main fatty acids in milk GM3 are C22:0 22%, C23:0 34% and C24:0 20% (manufacturer's data sheet). It is speculated that GM3 did not mix with DPPC due to the difference of the hydrophobic acyl chains. However, this is unlikely since the antibody binds preferentially synthetic C16:0 GM3/DPPC to C16:0 GM3/POPC, suggesting that C16:0 GM3 also phase separated from DPPC. Since pSM and C16:0 GM3 share hydrophobic ceramide moiety, hydrophilic carbohydrate moiety of GM3 may be involved in the different interaction of pSM and GM3 to DOPC and DPPC. Atomistic MD simulations of DOPC/Chol/SM (45/25/10) bilayers containing 20 mol % GM3 showed that GM3 interacted most strongly with themselves, followed by SM, DOPC and Chol [56]. Interestingly, 65% of the interaction energy of between GM3 is generated by interactions between headgroups [56].

Our results indicate that GM3 clusters were preferentially formed in less fluid membrane or at low temperature. Carbohydrate to carbohydrate interaction of GM3 may occur both in solid and fluid membranes. GM3 is reported to spontaneously transfer between membranes above T_m [57]. We speculate that spontaneous detachment and insertion of GM3 into DOPC-rich fluid regions of the membrane disturbs the stable formation of GM3 clusters (Fig. 5).

In contrast to GM1-cholera toxin interaction [17], the presence of cholesterol did not affect the binding of anti-GM3 antibody, GMR6, suggesting that cholesterol does not change the conformation of GM3. This may be due to the

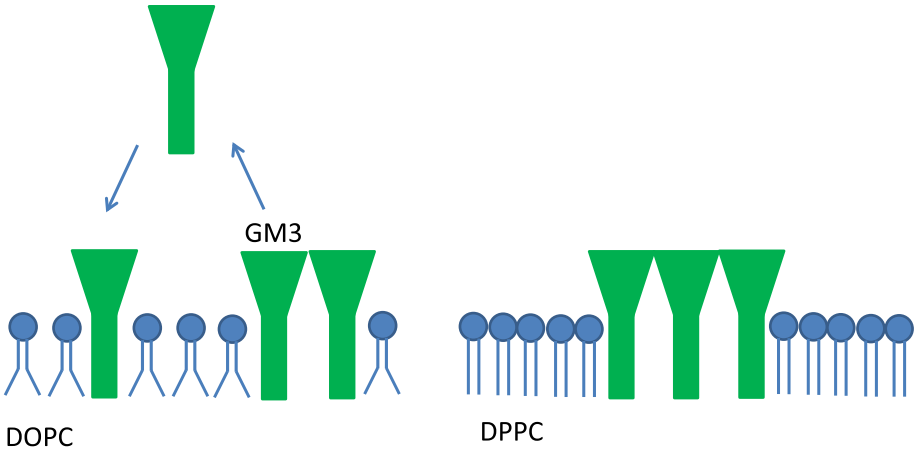

Fig. 5 Putative distribution of GM3 in DOPC and DPPC. Hydrogen bond between glycans facilitates clustering of GM3 both in DOPC and DPPC membrane. In DOPC, GM3 readily detaches from the membrane and then inserts into GM3-poor fluid DOPC-rich area. GM3 clusters are more stable in DPPC

relatively small headgroup of GM3 compared to GM1. This observation may be related to the MD simulation results [56] that GM1 and GM2 nanodomains were enlarged by cholesterol whereas the domain size of GM3 was not affected due to strong GM3-GM3 interaction.

Cell density dependent labeling of cellular GM3 by anti-GM3 antibody

Similar to ELISA results, the binding of anti-GM3 to cell surface GM3 showed temperature dependence. While cells were efficiently labeled at 4 ℃, labeling was less efficient at higher temperatures. These results suggest that the anti-GM3 antibody preferentially binds to GM3 in less fluid lipid environment.

It has long been known that in several cell types, anti-GM3 antibody labels sparse but not confluent cells [18, 19]. Since cell density does not affect GM3 content and GM3 can be chemically labeled in a cell-density-independent manner [18, 19], it is speculated that GM3 is cryptic in confluent cells. However, the molecular mechanism of the crypticity is not known. Confluent melanoma cells were not labeled with the antibody even at 4 ℃, suggesting strong differences in lipid distribution between sparse and confluent cells. Indeed, our FLIM experiments showed huge difference in lipid order in low density and high density cells.

Anti-GM3 antibodies added to the medium only labels the outer leaflet of the plasma membrane. Phospholipids are asymmetrically distributed in the plasma membrane [40] and the outer leaflet is enriched with sphingomyelin (88% in the outer leaflet in human skin fibroblasts) and phosphatidylcholine (92% in the outer leaflet) [25]. In contrast, more than 95% of phosphatidylethanolamine, phosphatidylinositol and phosphatidylserine are localized in the inner leaflet [25]. Our results using outer leaflet specific dye, F2N12S, indicate the alteration of physical properties of sphingomyelin and phosphatidylcholine-enriched outer leaflet of the plasma membrane between low and high density cells. Biochemical analysis of lipids indicates that the gross lipid composition and cholesterol content were not significantly altered between low density and high density cells. Cholesterol-binding D4 labeling suggests that cell surface cholesterol distribution is also similar between high and low density cells. Content and fatty acid composition of sphingomyelin were also not affected. In contrast, there were differences in phosphatidylcholine molecular species between low and high density cells. There were a decrease in DPPC and increases in mono- and di-unsaturated molecular species whereas polyunsaturated molecular species were decreased in high density cells. Although the molecular species of phospholipids in the outer and inner leaflet of red blood cells have been studied [41], lipidomics of the outer and inner leaflet of the plasma membrane from nucleated cells has not been reported. Plasma membrane phospholipids were estimated to be 13% of total cellular phospholipids in baby hamster kidney (BHK) cells [58]. Using different enveloped viruses, the enrichment of monounsaturated- and decrease of polyunsaturated-phosphatidylcholine in the plasma membrane in human skin fibroblasts are suggested [42]. Our results showed that the addition of oleic acid (C18:1) to low density cells abolished anti-GM3 labeling. Oleic acid is reported to be efficiently incorporated to phosphatidylcholine [51]. Our results suggest the role of monounsaturated molecular species of phosphatidylcholine in alteration of GM3 microenvironment.

It is reported that lipids are mobile even after paraformaldehyde fixation [34]. Thus we cannot inhibit the formation of pseudo-cluster of GM3 by multivalent IgM antibodies. However, our results indicate that the pre-existed lipid cluster is required for the binding of the antibody. In summary, our results suggested that anti-GM3 antibody bind to GM3 only when GM3 forms clusters. Formation of clusters is dependent on fatty acid composition of partner lipids both in model and cell membranes. Our results revealed that the crypticity of GM3 against anti-GM3 antibody is due to the

alteration of fatty acid composition of the surrounding lipids of GM3.

Methods

Antibodies

Anti-GM3 monoclonal IgM clones GMR6 and M2590 were obtained from TCI Europe (Zwijndrecht, Belgium) and Cosmo Bio (Tokyo, Japan), respectively. Anti-GM3 IgG clone DH2 was obtained as described [8]. HRP-labeled anti-mouse IgM was from Sigma (St Louis, MI). HRP-labeled anti-mouse IgG was from GE Healthcare (Chicago, Il). Alexa488-labeled anti-mouse IgM was from Molecular probes (Eugene, OR).

Lipids and other reagents

Glucosylceramide (Gaucher's spleen, GlcCer), lactosylceramide (bovine buttermilk, LacCer), N-acyl-sphingosylphosphorylethanolamine (bovine buttermilk, CerPE), monosialogangliosides, GM1 (Galβ1,3GalNAcβ1,4(Neu5Acα2,3) Galβ1,4Glcβ1,1'-ceramide) from bovine and GM3 (Neu5Acα2,3 Galβ1,4Glcβ1,1'-ceramide) from bovine buttermilk were from Matreya LLC (State College, PA). Major fatty acids of buttermilk GM3 were C16:0 6%, C22:0 22%, C23:0 34% and C24:0 20% according to the manufacturer. C8:0, C12:0, C16:0 and C24:0-GM3 were from Nagara Science (Gifu, Japan). The following lipids were purchased from Avanti Polar Lipids (Alabaster, AL): 1,2-dimyristoyl-*sn*-glycero-3-phosphocholine (DMPC), 1,2-dioleoyl-*sn*-glycero-3-phosphocholine (DOPC), 1,2-dipalmitoyl-*sn*-glycero-3-phosphocholine (DPPC), 1-palmitoyl-2-oleoyl-*sn*-glycero-3-phosphocholine (POPC), palmitoyl sphingomyelin (pSM), ceramide (porcine brain, Cer), 1,2-dipalmitoyl-*sn*-glycero-3-phosphoethanolamine (DPPE), 1,2-dioleoyl-*sn*-glycero-3-phosphoethanolamine (DOPE), 1,2-dioleoyl-*sn*-glycero-3-phospho-L-serine (DOPS), 1,2-dioleoyl-*sn*-glycero-3-phospho-(1'-rac-glycerol) (DOPG), 1',3'-bis[1,2-dioleoyl-*sn*-glycero-3-phospho]-glycerol (TOCL), C11 TopFluor-GM3. GM2 (GalNAcβ1,4(Neu5Acα2,3)Galβ1,4Glcβ1,1'-ceramide) from bovine brain was from Wako Pure Chemical Industries (Osaka, Japan). Lyso GM3 was provided by Sonnino's laboratory and prepared as described [59]. ATTO594-GM3 was prepared as described [28]. N-[[4'-N,N-diethylamino-3-hydroxy-6-flavonyl]-methyl]-N-methyl-N-(3-sulfopropyl)-1-dodecanaminium, inner salt (F2N12S) was prepared as described [36]. mCherry-D4 was prepared as described [60].

Enzyme-linked immunosorbent assay (ELISA)

ELISA was performed as described previously [61].

Surface plasmon resonance (SPR)

GM3-containing liposomes were prepared as follows: Fig. 1D: 50 nmol of GM3 in a chloroform/methanol (2:1) solution was mixed with either 250 nmol DOPC or DPPC in the same solvent and dried under nitrogen. Figure 1E, the solutions containing 250 nmol DPPC and 100 nmol GM3 with or without 250 nmol cholesterol were prepared. In Fig. 1F, 25 nmol of GM3 was mixed with 225 nmol DPPC. Dried samples were mixed vigorously in 200 µl of HBS-N buffer (10 mM Hepes, pH 7.4, 150 mM NaCl). GM3 containing liposomes were prepared by sonicating 5 min three times in bath sonicator. The initial temperature of the water bath was set at 41 ℃ (Fig. 1D and E) or room temperature (Fig. 1F). Alternatively, liposomes were frozen in liquid nitrogen and thawed at 50 ℃. This cycle was repeated three times. All conditions gave similar results. Liposome solutions were filtered through a 0.22 µmϕ polyvinylidene difluoride (PVDF, Millipore Co., Burlington, MA). These solutions were diluted ten times with HBS-N buffer, then immobilized on a biosensor L1 chip (Cytiba, Tokyo, Japan) at flow rate 10 µL/min. The chip surface was washed with 50 mM NaOH, then blocked with 100 µg/mL BSA in HBS-N buffer. Experiments were carried out at 25 ℃ at flow rate 10 µL/min (Fig. 1D and E) or 30 µL/min (Fig. 1F). The binding of the anti-GM3 antibody to GM3 was analyzed with a Biacore 3000 analytical system. Data were evaluated with the BIAevaluation 4.1.1 software program (Biacore, Cytiba). The results shown represent 3–4 independent experiments.

Fluorescence measurement of liposomes

Small unilamellar vesicles (SUVs) containing DPPC/C11 TopFluor-GM3/ATTO594-GM3 (99/0.5/0.5), DOPC/C11 TopFluor-GM3/ATTO594-GM3 (99/0.5/0.5), DPPC/ATTO594-GM3 (99.5/0.5), DOPC/ATTO594-GM3 (99.5/0.5) were prepared in PBS by ethanol injection [62, 63]. Fluorescence spectra measurements were recorded with a Fluoromax Plus spectrofluorometer (Horiba Jobin–Yvon, Lille, France) equipped with a thermostat cell compartment. To solubilize lipids, Triton X-100 (final concentration 1%) was added. FRET efficiency was calculated as

$$\left(\text{Emission of donor } \left(F_{507}\right) \text{ in the absence of acceptor} - \text{Emission of donor } \left(F_{507}\right) \text{ in the presence of acceptor}\right) / \text{Emission of donor } \left(F_{507}\right) \text{ in the absence of acceptor} \quad (1)$$

or

$$\left(\text{Emission of donor } \left(F_{507}\right) + \text{ Emission of acceptor } \left(F_{626}\right)\right) / \text{Emission of donor } \left(F_{507}\right) \quad (2)$$

Cells

Human embryonic kidney cell line, HEK293 was grown in Dulbecco's modified Eagle's medium (DMEM) supplemented with 10% fetal calf serum, 1% L-glutamine, 100 units/mL penicillin and 100 µg/mL streptomycin. Mouse melanoma cell line, MEB4 was cultured as described [64]. Human skin fibroblasts were grown as described [65]. Niemann-Pick A fibroblasts were grown as described [66].

Antibody labeling of cells

HEK293 cells were grown on a plastic bottom dish (Ibidi, Gräfelfing, Germany), and MEB4 cells, human skin fibroblasts, and NPA fibroblasts were grown on glass coverslips to 30–40% confluent and fixed with 4% paraformaldehyde in PBS for 20 min at room temperature. Cells were then blocked with 3% BSA in PBS for 1 h, pre-warmed for 20 min at indicated temperatures, and labeled with 22.4 µg/ml anti-GM3 antibody, GMR6, for 1 h at indicated temperatures, followed by incubation with Alexa488-labeled anti-mouse IgM secondary antibody for 1 h. After washing with PBS, the coverslips were mounted with ProLong Diamond antifade mountant (Invitrogen, Carlsbad, CA). The specimens were observed under an LSM700 confocal microscope (Zeiss, Oberkochen, Germany).

To obtain low and high densities MEB4 cell line, cells were seeded on the glass coverslips at 30–40% in low density and 90–120% in high density. After culturing overnight, cell densities were examined under a light microscope (Nikon, Tokyo, Japan). Cells were fixed with 4% paraformaldehyde in PBS for 20 min at room temperature, blocked with 3% BSA in PBS for 1 h, pre-warmed for 20 min at different temperatures, and then labeled with 22.4 µg/ml anti-GM3 antibody for 1 h at indicated temperatures, followed by incubation with Alexa488-labeled anti-mouse IgM secondary antibody for 1 h. After washing with PBS, actin fibers were stained with Alexa594-labeled phalloidin (Molecular Probes) as described [18]. The coverslips were mounted with ProLong Diamond antifade mountant. The specimens were observed under an LSM700 confocal microscope.

Confocal microscopy

Stained cells were imaged using an LSM700 confocal microscope equipped with a C-Apochromat 63XW Korr (1.2 NA) objective.

Fluorescence lifetime imaging microscopy (FLIM)

Sparse and confluent MEB4 cells were washed with PBS and then stained by adding a freshly prepared solution of F2N12S in PBS to a final concentration of 0.1 µM per 10^6 cells (< 0.25% DMSO volume), and incubated for 2 min in the dark at room temperature [37]. The cells were then washed again with PBS before measurement. We performed two-photon fluorescence microscopy at 25 ℃ by using an in-house-built two-photon laser scanning setup based on an inverted microscope (IX70, Olympus, Tokyo, Japan) with an 60 × 1.2NA water immersion objective (UPlan-Apo, Olympus) and two fast galvo mirrors in the descanned fluorescence collection mode [67, 68]. Two-photon excitation was provided by a femtosecond laser (Insight DeepSee, Spectra Physics, Milpitas, CA). The typical excitation power was ~ 2.5 mW (λ = 830 nm) at the sample. Photons were detected using an avalanche photodiode (SPCM-AQR-14-FC; Perkin Elmer) coupled to an HQ 585/40 bandpass filter and a single photon-counting TCSPC module (SPC830, Becker & Hickl, Berlin, Germany) operating in the reversed start-stop mode. Acquisition times were adjusted to achieve 1000 photons per pixel. The minimum fluorescence lifetime detectable with this setup is ~ 300 ps.

FLIM data were analyzed using the FLIMfit software (Imprerial College London) [69]. The images were initially segmented to analyze only data from plasma membranes. The lifetimes were recovered from the fluorescence decay using an iterative reconvolution method [70]. The goodness of the fit was evaluated from the χ^2 values, which ranged from 0.9 to 1.2, and from the plot of the distribution of the residuals.

mCherry-D4 labeling

Low density and high density MEB4 cells were prepared as described above. Cell surface mCherry-D4 labeling was performed as described [71].

Oleic acid treatment of low density MEB4 cells

MEB4 cells were grown in glass-bottom dish to low density. The medium was exchanged to serum-free medium containing 0.4% BSA and 500 µM oleic acid. After 1 h or 2 h incubation at 37 ℃, cells were fixed and labeled with anti-GM3 antibody as described above.

Lipid analyses

The same numbers of MEB4 cells were cultured in 15 cm (low density) and 3.5 cm (high density) dishes, respectively. Cells were washed three times with ice-cold PBS, scraped, washed three times again in ice-cold PBS, and divided to one

portion for protein determination and nine portions for lipid extraction. For protein determination, cells were collected by centrifugation, lysed by vortex in 0.1% Triton X-100, 2 mM EDTA in Milli Q (pH 7.4), and fragmented using probe sonicator for 1 min, followed by freeze-thawing. Protein contents were measured using a BCA protein assay kit (ThermoFisher Scientific, Waltham, MA). For lipid extraction, cells were collected by centrifugation and extracted lipids with chloroform/methanol (1:2 by vol., and then 2:1 by vol.). Lipids were applied to HPTLC plates (Merck, Darmstadt, Germany) by adjusting with protein contents. The plates were developed sequentially in (1) chloroform/methanol/formic acid/water (65:25:8.9:1.1 by vol.), (2) chloroform/methanol/4.4 M ammonia (50:40:10 by vol.), and (3) diethylether [39, 72]. Glycolipids were visualized by spraying orcinol reagent and heating at 100 ℃ while phospholipids and neutral lipids were visualized by spraying cupric acetate solution to the same plates and heating at 180 ℃. The position of each lipid on HPTLC was determined using lipid standards.

For the detection of phospholipid molecular species, cells were prepared as described above and LC/ESI–MS-based lipidomics analyses were performed on a Shimadzu Nexera UPLC system (Shimadzu, Kyoto, Japan) coupled with a QTRAP 4500 hybrid triple quadrupole linear ion trap mass spectrometer (AB Sciex, Framingham, MA). Lipids extracted from melanoma cells [73] were injected by an auto sampler. Chromatographic separation was performed on a SeQuant ZIC-HILIC PEEK coated column (250 mm × 2.1 mm, 1.8 µm; Millipore) maintained at 50 ℃ using mobile phase A (water/acetonitrile (95/5, v/v) containing 10 mM ammonium acetate) and mobile phase B (water/acetonitrile (50/50, v/v) containing 20 mM ammonium acetate) in a gradient programme (0–22 min: 0% B → 40% B; 22–25 min: 40% B → 40% B; 25–30 min: 0% B) with a flow rate of 0.5 mL/min. The instrument parameters for negative ion mode were as follows: curtain gas, 10 psi; collision gas, 7 arb. unit; ionspray voltage, − 4500 V; temperature, 700 ℃; ion source gas 1, 30 psi; ion source gas 2, 70 psi. Detection of phospholipid species was performed by multiple reaction monitoring (MRM) as described in Supplemental Table 1.

Supplementary Information The online version contains supplementary material available at https://doi.org/10.1007/s00018-023-04813-9.

Author contributions Conceptualization, TK; methodology, LR, NH and JA; investigation, MM, NY, NT, LR, BP, AM and NK; resources LM, SS, NK, HA, MKK, YK, KI and JI; writing—original draft, MM and TK; writing—review and editing, MM, NT, LR, NH, NK, JA, YS, SS, JI, YM, KI and TK; supervision, JI, KI, YM and TK.

Funding Mizutani Foundation for Glycoscience (to N.Y. and T.K). RIKEN Glycolipidologue Initiative Program (to T.K. and Y.S.). Vaincre les Maladies Lysosomales (19/LBPH/S44 to T.K.) Japan Agency for Medical Reasearch and Development (AMED) (JP22ama121008 and JP22am0401013 to Y.K.) Agence Nationale pour la Recherche (ANR-19-CE16-0012-02 and ANR-22-CE44-0019-01 to T.K.). ITMO Cancer of Aviesan within the framework of the 2021–2030 Cancer Control Strategy, on funds administered by Inserm (to T.K.). Y.M. is grateful to the Institut Universitaire de France (IUF) for financial support and providing additional time to be dedicated to research.

Data and materials availability The datasets generated and/or analyzed during the current study are available from the corresponding author on reasonable request.

Declarations

Conflict of interest Authors declare that they have no competing interests.

Ethical approval and consent to participate Not applicable.

Consent for publication All authors agreed on the final version of the manuscript.

References

1. Zheng M, Fang H, Tsuruoka T, Tsuji T, Sasaki T, Hakomori S (1993) Regulatory role of GM3 ganglioside in alpha 5 beta 1 integrin receptor for fibronectin-mediated adhesion of FUA169 cells. J Biol Chem 268(3):2217–2222. https://doi.org/10.1016/S0021-9258(18)53984-3
2. Kabayama K, Sato T, Saito K, Loberto N, Prinetti A, Sonnino S, Kinjo M, Igarashi Y, Inokuchi J (2007) Dissociation of the insulin receptor and caveolin-1 complex by ganglioside GM3 in the state of insulin resistance. Proc Natl Acad Sci USA 104(34):13678–13683. https://doi.org/10.1073/pnas.0703650104
3. Coskun U, Grzybek M, Drechsel D, Simons K (2011) Regulation of human EGF receptor by lipids. Proc Natl Acad Sci USA 108(22):9044–9048. https://doi.org/10.1073/pnas.1105666108
4. Nakano M, Hanashima S, Hara T, Kabayama K, Asahina Y, Hojo H, Komura N, Ando H, Nyholm TKM, Slotte JP, Murata M (2021) FRET detects lateral interaction between transmembrane domain of EGF receptor and ganglioside GM3 in lipid bilayers. Biochim Biophys Acta 1863:183623. https://doi.org/10.1016/j.bbamem.2021.183623
5. Inokuchi JI, Kanoh H, Inamori KI, Nagafuku M, Nitta T, Fukase K (2021) Homeostatic and pathogenic roles of the GM3 ganglioside. FEBS J 289:5152–5165. https://doi.org/10.1111/febs.16076
6. Hirabayashi Y, Hamaoka A, Matsumoto M, Matsubara T, Tagawa M, Wakabayashi S, Taniguchi M (1985) Syngeneic monoclonal antibody against melanoma antigen with interspecies cross-reactivity recognizes GM3, a prominent ganglioside of B16 melanoma. J Biol Chem 260(24):13328–13333. https://doi.org/10.1016/S0021-9258(17)38873-7
7. Kotani M, Ozawa H, Kawashima I, Ando S, Tai T (1992) Generation of one set of monoclonal antibodies specific for a-pathway ganglio-series gangliosides. Biochim Biophys Acta 1117(1):97–103. https://doi.org/10.1016/0304-4165(92)90168-t
8. Dohi T, Nores G, Hakomori S (1988) An IgG3 monoclonal antibody established after immunization with GM3 lactone: immunochemical specificity and inhibition of melanoma cell growth in vitro and in vivo. Cancer Res 48:5680–5685
9. Gomez-Mouton C, Abad JL, Mira E, Lacalle RA, Gallardo E, Jimenez-Baranda S, Illa I, Bernad A, Manes S, Martinez AC (2001) Segregation of leading-edge and uropod components into specific lipid rafts during T cell polarization. Proc Natl Acad Sci USA 98:9642–9647. https://doi.org/10.1073/pnas.171160298

10. Janich P, Corbeil D (2007) GM1 and GM3 gangliosides highlight distinct lipid microdomains within the apical domain of epithelial cells. FEBS Lett 581:1783–1787. https://doi.org/10.1016/j.febslet.2007.03.065
11. Fujita A, Cheng J, Hirakawa M, Furukawa K, Kusunoki S, Fujimoto T (2007) Gangliosides GM1 and GM3 in the living cell membrane form clusters susceptible to cholesterol depletion and chilling. Mol Biol Cell 18:2112–2122. https://doi.org/10.1091/mbc.e07-01-00712
12. Chigorno V, Palestini P, Sciannamblo M, Dolo V, Pavan A, Tettamanti G, Sonnino S (2000) Evidence that ganglioside enriched domains are distinct from caveolae in MDCK II and human fibroblast cells in culture. Eur J Biochem 267(13):4187–4197. https://doi.org/10.1046/j.1432-1327.2000.01454.x
13. Cutillo G, Saariaho AH, Meri S (2020) Physiology of gangliosides and the role of antiganglioside antibodies in human diseases. Cell Mol Immunol 17:313–322. https://doi.org/10.1038/s41423-020-0388-9
14. Willison HJ, Yuki N (2002) Peripheral neuropathies and anti-glycolipid antibodies. Brain 125:2591–2625. https://doi.org/10.1093/brain/awf272
15. Lloyd KO, Gordon CM, Thampoe IJ, DiBenedetto C (1992) Cell surface accessibility of individual gangliosides in malignant melanoma cells to antibodies is influenced by the total ganglioside composition of the cells. Cancer Res 52:4948–4953
16. Greenshields KN, Halstead SK, Zitman FM, Rinaldi S, Brennan KM, O'Leary C, Chamberlain LH, Easton A, Roxburgh J, Pediani J, Furukawa K, Furukawa K, Goodyear CS, Plomp JJ, Willison HJ (2009) The neuropathic potential of anti-GM1 autoantibodies is regulated by the local glycolipid environment in mice. J Clin Invest 119:595–610. https://doi.org/10.1172/JCI37338
17. Lingwood D, Binnington B, Rog T, Vattulainen I, Grzybek M, Coskun U, Lingwood CA, Simons K (2011) Cholesterol modulates glycolipid conformation and receptor activity. Nat Chem Biol 7:260–262. https://doi.org/10.1038/nchembio.551
18. Sakiyama H, Takahashi T, Hirabayashi Y, Taniguchi M (1987) Change in the topographical distribution of GM3 during cell spreading and growth: immunostaining with monoclonal antibody against GM3. Cell Struct Funct 12:93–105. https://doi.org/10.1247/csf.12.93
19. Tatewaki K, Yamaki T, Maeda Y, Tobioka H, Piao H, Yu H, Ibayashi Y, Sawada N, Hashi K (1997) Cell density regulates crypticity of GM3 ganglioside on human glioma cells. Exp Cell Res 233:145–154. https://doi.org/10.1006/excr.1997.3563
20. Kotani M, Kawashima I, Ozawa H, Ogura K, Ishizuka I, Terashima T, Tai T (1994) Immunohistochemical localization of minor gangliosides in the rat central nervous system. Glycobiology 4:855–865. https://doi.org/10.1093/glycob/4.6.855
21. Sorice M, Parolini I, Sansolini T, Garofalo T, Dolo V, Sargiacomo M, Tai T, Peschle C, Torrisi MR, Pavan A (1997) Evidence for the existence of ganglioside-enriched plasma membrane domains in human peripheral lymphocytes. J Lipid Res 38:969–980. https://doi.org/10.1016/S0022-2275(20)37221-7
22. Misasi R, Sorice M, Garofalo T, Griggi T, Campana WM, Giammatteo M, Pavan A, Hiraiwa M, Pontieri GM, O'Brien JS (1998) Colocalization and complex formation between prosaposin and monosialoganglioside GM3 in neural cells. J Neurochem 71:2313–2321. https://doi.org/10.1046/j.1471-4159.1998.71062313.x
23. Garofalo T, Lenti L, Longo A, Misasi R, Mattei V, Pontieri GM, Pavan A, Sorice M (2002) Association of GM3 with Zap-70 induced by T cell activation in plasma membrane microdomains: GM3 as a marker of microdomains in human lymphocytes. J Biol Chem 277:11233–11238. https://doi.org/10.1074/jbc.M109601200
24. Chen Y, Qin J, Chen ZW (2008) Fluorescence-topographic NSOM directly visualizes peak-valley polarities of GM1/GM3 rafts in cell membrane fluctuations. J Lipid Res 49:2268–2275. https://doi.org/10.1194/jlr.D800031-JLR200
25. Murate M, Abe M, Kasahara K, Iwabuchi K, Umeda M, Kobayashi T (2015) Transbilayer distribution of lipids at nano scale. J Cell Sci 128:1627–1638. https://doi.org/10.1242/jcs.163105
26. Marsh D (2013) Handbook of lipid bilayers, 2nd edn. CRC Press, Boca Raton
27. Taniguchi M, Wakabayashi S (1984) Shared antigenic determinant expressed on various mammalian melanoma cells. Gan 75:418–426
28. Komura N, Suzuki KG, Ando H, Konishi M, Koikeda M, Imamura A, Chadda R, Fujiwara TK, Tsuboi H, Sheng R, Cho W, Furukawa K, Furukawa K, Yamauchi Y, Ishida H, Kusumi A, Kiso M (2016) Raft-based interactions of gangliosides with a GPI-anchored receptor. Nat Chem Biol 12:402–410. https://doi.org/10.1038/nchembio.2059
29. MacDonald RI (1990) Characteristics of self-quenching of the fluorescence of lipid-conjugated rhodamine in membranes. J Biol Chem 265:13533–13539. https://doi.org/10.1016/S0021-9258(18)77380-77388
30. Elvington SM, Nichols JW (2007) Spontaneous, intervesicular transfer rates of fluorescent, acyl chain-labeled phosphatidylcholine analogs. Biochim Biophys Acta 1768:502–508. https://doi.org/10.1016/j.bbamem.2006.11.013
31. Coste V, Puff N, Lockau D, Quinn PJ, Angelova MI (2006) Raft-like domain formation in large unilamellar vesicles probed by the fluorescent phospholipid analogue, C12NBD-PC. Biochim Biophys Acta 1758:460–467. https://doi.org/10.1016/j.bbamem.2006.03.003
32. Puff N, Watanabe C, Seigneuret M, Angelova MI, Staneva G (2014) Lo/Ld phase coexistence modulation induced by GM1. Biochim Biophys Acta 1838:2105–2114. https://doi.org/10.1016/j.bbamem.2014.05.002
33. Xu X, London E (2000) The effect of sterol structure on membrane lipid domains reveals how cholesterol can induce lipid domain formation. Biochemistry 39(5):843–849. https://doi.org/10.1021/bi992543v
34. Tanaka KA, Suzuki KG, Shirai YM, Shibutani ST, Miyahara MS, Tsuboi H, Yahara M, Yoshimura A, Mayor S, Fujiwara TK, Kusumi A (2010) Membrane molecules mobile even after chemical fixation. Nat Methods 7:865–866. https://doi.org/10.1038/nmeth.f.314
35. Brady RO, Kanfer JN, Mock MB, Fredrickson DS (1966) The metabolism of sphingomyelin. II. Evidence of an enzymatic deficiency in Niemann-Pick diseaese. Proc Natl Acad Sci USA 55:366–369. https://doi.org/10.1073/pnas.55.2.366
36. Shynkar VV, Klymchenko AS, Kunzelmann C, Duportail G, Muller CD, Demchenko AP, Freyssinet JM, Mely Y (2007) Fluorescent biomembrane probe for ratiometric detection of apoptosis. J Am Chem Soc 129(7):2187–2193. https://doi.org/10.1021/ja068008h
37. Kilin V, Glushonkov O, Herdly L, Klymchenko A, Richert L, Mely Y (2015) Fluorescence lifetime imaging of membrane lipid order with a ratiometric fluorescent probe. Biophys J 108:2521–2531. https://doi.org/10.1016/j.bpj.2015.04.003
38. Shimada Y, Maruya M, Iwashita S, Ohno-Iwashita Y (2002) The C-terminal domain of perfringolysin O is an essential cholesterol-binding unit targeting to cholesterol-rich microdomains. Eur J Biochem 269:6195–6203. https://doi.org/10.1046/j.1432-1033.2002.03338.x
39. Kishimoto T, Tomishige N, Murate M, Ishitsuka R, Schaller H, Mely Y, Ueda K, Kobayashi T (2020) Cholesterol asymmetry at the tip of filopodia during cell adhesion. FASEB J 34:6185–6197. https://doi.org/10.1096/fj.201900065RR

40. Verkleij AJ, Zwaal RF, Roelofsen B, Comfurius P, Kastelijn D, van Deenen LL (1973) The asymmetric distribution of phospholipids in the human red cell membrane. A combined study using phospholipases and freeze-etch electron microscopy. Biochim Biophys Acta 323:178–193. https://doi.org/10.1016/0005-2736(73)90143-0
41. Doktorova M, Symons JL, Levental I (2020) Structural and functional consequences of reversible lipid asymmetry in living membranes. Nat Chem Biol 16:1321–1330. https://doi.org/10.1038/s41589-020-00688-0
42. Blom TS, Koivusalo M, Kuismanen E, Kostiainen R, Somerharju P, Ikonen E (2001) Mass spectrometric analysis reveals an increase in plasma membrane polyunsaturated phospholipid species upon cellular cholesterol loading. Biochemistry 40:14635–14644. https://doi.org/10.1021/bi0156714
43. Samuel D, Paris S, Ailhaud G (1976) Uptake and metabolism of fatty acids and analogues by cultured cardiac cells from chick embryo. Eur J Biochem 64:583–595. https://doi.org/10.1111/j.1432-1033.1976.tb10338.x
44. Rohwedder A, Zhang Q, Rudge SA, Wakelam MJ (2014) Lipid droplet formation in response to oleic acid in Huh-7 cells is mediated by the fatty acid receptor FFAR4. J Cell Sci 127:3104–3115. https://doi.org/10.1242/jcs.145854
45. Targett-Adams P, Chambers D, Gledhill S, Hope RG, Coy JF, Girod A, McLauchlan J (2003) Live cell analysis and targeting of the lipid droplet-binding adipocyte differentiation-related protein. J Biol Chem 278:15998–16007. https://doi.org/10.1074/jbc.M211289200
46. Wang H, Wei E, Quiroga AD, Sun X, Touret N, Lehner R (2010) Altered lipid droplet dynamics in hepatocytes lacking triacylglycerol hydrolase expression. Mol Biol Cell 21:1991–2000. https://doi.org/10.1091/mbc.e09-05-0364
47. Homan R, Grossman JE, Pownall HJ (1991) Differential effects of eicosapentaenoic acid and oleic acid on lipid synthesis and secretion by HepG2 cells. J Lipid Res 32:231–241. https://doi.org/10.1016/S0022-2275(20)42084-X
48. Schroedl NA, Hartzell CR (1984) Preferential distribution of non-esterified fatty acids to phosphatidylcholine in the neonatal mammalian myocardium. Biochem J 224:651–659. https://doi.org/10.1042/bj2240651
49. Wang S, McLeod RS, Gordon DA, Yao Z (1996) The microsomal triglyceride transfer protein facilitates assembly and secretion of apolipoprotein B-containing lipoproteins and decreases cotranslational degradation of apolipoprotein B in transfected COS-7 cells. J Biol Chem 271:14124–14133. https://doi.org/10.1074/jbc.271.24.14124
50. Caviglia JM, De Gomez Dumm IN, Coleman RA, Igal RA (2004) Phosphatidylcholine deficiency upregulates enzymes of triacylglycerol metabolism in CHO cells. J Lipid Res 45:1500–1509. https://doi.org/10.1194/jlr.M400079-JLR200
51. Besson N, Hullin-Matsuda F, Makino A, Murate M, Lagarde M, Pageaux JF, Kobayashi T, Delton-Vandenbroucke I (2006) Selective incorporation of docosahexaenoic acid into lysobisphosphatidic acid in cultured THP-1 macrophages. Lipids 41:189–196. https://doi.org/10.1007/s11745-006-5087-5
52. Maggio B, Ariga T, Sturtevant JM, Yu RK (1985) Thermotropic behavior of binary mixtures of dipalmitoylphosphatidylcholine and glycosphingolipids in aqueous dispersions. Biochim Biophys Acta 818:1–12. https://doi.org/10.1016/0005-2736(85)90131-2
53. Matuoka S, Akiyama M, Yamada H, Tsuchihashi K, Gasa S (2003) Phase behavior in multilamellar vesicles of DPPC containing ganglioside GM3 with a C18:1 sphingoid base and a 24:0 acyl chain (GM3(18,24)) observed by X-ray diffraction. Chem Phys Lipids 123:19–29. https://doi.org/10.1016/s0009-3084(02)00128-7
54. Maggio B, Ariga T, Sturtevant JM, Yu RK (1985) Thermotropic behavior of glycosphingolipids in aqueous dispersions. Biochemistry 24:1084–1092. https://doi.org/10.1016/0005-2736(85)90131-2
55. Maulik PR, Shipley GG (1996) N-palmitoyl sphingomyelin bilayers: structure and interactions with cholesterol and dipalmitoylphosphatidylcholine. Biochemistry 35:8025–8034. https://doi.org/10.1021/bi9528356
56. Sarmento MJ, Owen MC, Ricardo JC, Chmelova B, Davidovic D, Mikhalyov I, Gretskaya N, Hof M, Amaro M, Vacha R, Sachl R (2021) The impact of the glycan headgroup on the nanoscopic segregation of gangliosides. Biophys J 120:5530–5543. https://doi.org/10.1016/j.bpj.2021.11.017
57. Palestini P, Pitto M, Sonnino S, Omodeo-Sale MF, Masserini M (1995) Spontaneous transfer of GM3 ganglioside between vesicles. Chem Phys Lipids 77:253–260. https://doi.org/10.1016/0009-3084(95)02474-w
58. Brotherus J, Renkonen O (1977) Phospholipids of subcellular organelles isolated from cultured BHK cells. Biochim Biophys Acta 486:243–253. https://doi.org/10.1016/0005-2760(77)90020-0
59. Valiente O, Mauri L, Casellato R, Fernandez LE, Sonnino S (2001) Preparation of deacetyl-, lyso-, and deacetyl-lyso-GM(3) by selective alkaline hydrolysis of GM3 ganglioside. J Lipid Res 42(8):1318–1324. https://doi.org/10.1016/S0022-2275(20)31583-2
60. Abe M, Makino A, Hullin-Matsuda F, Kamijo K, Ohno-Iwashita Y, Hanada K, Mizuno H, Miyawaki A, Kobayashi T (2012) A role for sphingomyelin-rich lipid domains in the accumulation of phosphatidylinositol 4,5-bisphosphate to the cleavage furrow during cytokinesis. Mol Cell Biol 32:1396–1407. https://doi.org/10.1128/MCB.06113-11
61. Yamaji-Hasegawa A, Makino A, Baba T, Senoh Y, Kimura-Suda H, Sato SB, Terada N, Ohno S, Kiyokawa E, Umeda M, Kobayashi T (2003) Oligomerization and pore formation of a sphingomyelin-specific toxin, lysenin. J Biol Chem 278(25):22762–22770. https://doi.org/10.1074/jbc.M213209200
62. Kremer JM, Esker MW, Pathmamanoharan C, Wiersema PH (1977) Vesicles of variable diameter prepared by a modified injection method. Biochemistry 16:3932–3935. https://doi.org/10.1021/bi00636a033
63. Kobayashi T, Pagano RE (1988) ATP-dependent fusion of liposomes with the Golgi apparatus of perforated cells. Cell 55:797–805. https://doi.org/10.1016/0092-8674(88)90135-3
64. Ishitsuka R, Yamaji-Hasegawa A, Makino A, Hirabayashi Y, Kobayashi T (2004) A lipid-specific toxin reveals heterogeneity of sphingomyelin-containing membranes. Biophys J 86:296–307. https://doi.org/10.1016/S0006-3495(04)74105-3
65. Kobayashi T, Beuchat MH, Lindsay M, Frias S, Palmiter RD, Sakuraba H, Parton RG, Gruenberg J (1999) Late endosomal membranes rich in lysobisphosphatidic acid regulate cholesterol transport. Nat Cell Biol 1:113–118. https://doi.org/10.1038/10084
66. Makino A, Abe M, Murate M, Inaba T, Yilmaz N, Hullin-Matsuda F, Kishimoto T, Schieber NL, Taguchi T, Arai H, Anderluh G, Parton RG, Kobayashi T (2015) Visualization of the heterogeneous membrane distribution of sphingomyelin associated with cytokinesis, cell polarity, and sphingolipidosis. FASEB J 29:477–493. https://doi.org/10.1096/fj.13-247585
67. Clamme JP, Azoulay J, Mely Y (2003) Monitoring of the formation and dissociation of polyethylenimine/DNA complexes by two photon fluorescence correlation spectroscopy. Biophys J 84:1960–1968. https://doi.org/10.1016/S0006-3495(03)75004-8
68. Azoulay J, Clamme JP, Darlix JL, Roques BP, Mely Y (2003) Destabilization of the HIV-1 complementary sequence of TAR by the nucleocapsid protein through activation of

conformational fluctuations. J Mol Biol 326:691–700. https://doi.org/10.1016/s0022-2836(02)01430-4
69. Warren SC, Margineanu A, Alibhai D, Kelly DJ, Talbot C, Alexandrov Y, Munro I, Katan M, Dunsby C, French PM (2013) Rapid global fitting of large fluorescence lifetime imaging microscopy datasets. PLoS ONE 8:e70687. https://doi.org/10.1371/journal.pone.0070687
70. Becker W, Shcheslavkiy V, Frere S, Slutsky I (2014) Spatially resolved recording of transient fluorescence-lifetime effects by line-scanning TCSPC. Microsc Res Tech 77(3):216–224. https://doi.org/10.1002/jemt.22331
71. Yamaji-Hasegawa A, Murate M, Inaba T, Dohmae N, Sato M, Fujimori F, Sako Y, Greimel P, Kobayashi T (2022) A novel sterol-binding protein reveals heterogeneous cholesterol distribution in neurite outgrowth and in late endosomes/lysosomes. Cellul Mol Life Sci 79:324. https://doi.org/10.1007/s00018-022-04339-6
72. Yokoyama K, Suzuki M, Kawashima I, Karasawa K, Nojima S, Enomoto T, Tai T, Suzuki A, Setaka M (1997) Changes in composition of newly synthesized sphingolipids of HeLa cells during the cell cycle – suppression of sphingomyelin and higher-glycosphingolipid synthesis and accumulation of ceramide and glucosylceramide in mitotic cells. Eur J Biochem 249:450–455. https://doi.org/10.1111/j.1432-1033.1997.00450.x
73. Bligh EG, Dyer WJ (1959) A rapid method of total lipid extraction and purification. Can J Biochem Physiol 37:911–917. https://doi.org/10.1139/o59-099